Stratified construction of neural network based interatomic models for multicomponent materials

Samad Hajinazar, Junping Shao, and Aleksey N. Kolmogorov

Phys. Rev. B **95**, 014114 — Published 30 January 2017

DOI: 10.1103/PhysRevB.95.014114

Stratified construction of neural network-based interatomic models for multicomponent materials

Samad Hajinazar, Junping Shao, Aleksey N. Kolmogorov
Department of Physics, Applied Physics and Astronomy, Binghamton University, State University of New York, PO Box 6000, Binghamton, New York 13902-6000, USA
(Dated: November 9, 2016)

Recent application of neural networks (NNs) to modeling interatomic interactions has shown the learning machines' encouragingly accurate performance for select elemental and multicomponent systems. In this study, we explore the possibility of building a library of NN-based models by introducing a hierarchical NN training. In such a stratified procedure NNs for multicomponent systems are obtained by sequential training from the bottom up: first unaries, then binaries, and so on. Advantages of constructing NN sets with shared parameters include acceleration of the training process and intact description of the constituent systems. We use an automated generation of diverse structure sets for NN training on density functional theory-level reference energies. In the test case of Cu, Pd, Ag, Cu-Pd, Cu-Ag, Pd-Ag, and Cu-Pd-Ag systems, NNs trained in the traditional and stratified fashions are found to have essentially identical accuracy for defect energies, phonon dispersions, formation energies, etc. The models' robustness is further illustrated via unconstrained evolutionary structure searches in which the NN is used for the local optimization of crystal unit cells.

I. INTRODUCTION

Materials modeling and design require a toolset of diverse methods capable of describing relevant bonding, electronic, magnetic, optical, and other properties. In particular, reliable determination of materials' thermodynamic stability in structure searches or examination of materials' behavior in molecular dynamics simulations depend on accurate and efficient evaluation of the total energy and atomic forces. Given ionic positions, these basic quantities can be found at different levels of approximation with only partial or no explicit treatment of the electronic degrees of freedom. Striking a good balance between computational cost and approximation accuracy is one of the central goals in methodology development for materials research [1–10].

Density functional theory (DFT), based on parameterized functionals of the electron charge density, represents a reliable practical solution for establishing crystal structure stability for ordered phases with up to a few hundred atoms. Extensive benchmark studies have shown that $T = 0$ K total energy calculations at the (semi)local DFT approximation level correctly predict inorganic compound stability in 97% of metal-metal [11] and 83% of more complex metal-boron binaries [12]. Due to the costly N^3 scaling of DFT with system size, global ground state structure searches for systems exceeding several dozen atoms or simulations of phenomena extending over a few nm in size and/or several fs in time are prohibitively expensive.

The traditional construction of system- or interaction-specific classical models relies on the physical/chemical understanding of the bonding mechanisms. Families of bond-order potentials (BOPs), embedded-atom models (EAM), polarizable ion potentials, and Lennard-Jones potentials have been developed to treat systems with dominant covalent, metallic, ionic, and van der Waals types of interaction, respectively [13–18]. The main advantage of this approach is a relatively small number of semi-empirical fitting parameters but the rigid functional forms may in some cases fail to capture the full spectrum of many-body effects [19–21].

An alternative strategy for describing materials properties involves interpolation of large databases of DFT energies, forces, density of states (DOS), etc. [22–33]. Artificial neural networks (NNs) have proven to be effective machine learning tools for dealing with multidimensional classification, control, and interpolation problems in various fields. NNs were first used to map interatomic potential energy surfaces over two decades ago. As reviewed by Witkoskie and Doren [34], the early studies included parameterization of specific terms in known potentials or selected geometries. In Ref. 35 radial basis function-based NNs trained on energies and optionally forces showed good performance describing graphitic configurations with constant numbers of neighbors once the atomic environments were broken up into smaller collections of first and second nearest neighbors. Since NNs require a fixed number of input components, applicability of these early models was restricted to specific geometries or covalent framework types.

Major advances made in recent years have helped overcome this limitation. Behler and Parrinello [36] and Bartok *et al.* [23] have introduced so-called descriptors that enable fixed-size interaction-independent representations of arbitrary atomic environments. Use of these descriptors to preprocess atomic configurations into inputs for NNs was found to be effective in select Na, Cu, Si, W, H_2O, Cu-ZnO, and other systems [36–40]. Challenges and advances in constructing descriptors are detailed in several excellent reviews [2, 23, 41].

In this study we focus on two separate aspects of pro-

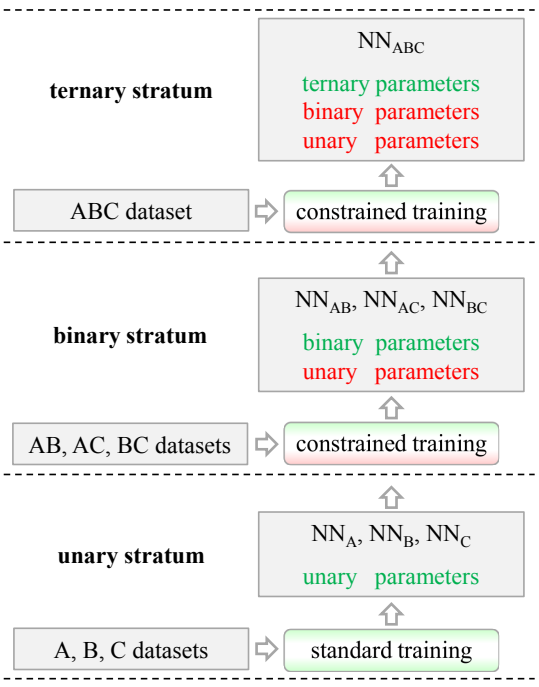

FIG. 1: (Color online) A flowchart demonstrating what data sets are used as well as what parameters are adjusted (in green) and fixed (in red) in the stratified training for a ternary system with elements A, B, and C. The ternary NN at the top inherits parameters from the constituent unary and binary systems. More details are given in Section V.

ducing practical NN-based models for multicomponent systems. First, we employ an automated structure generation scheme based on an evolutionary selection procedure that samples parts of the configurational space typically accessed in global structure searches. Second, we introduce and test a stratified training scheme as a basis for constructing extended NN libraries for multicomponent systems. Fig. 1 shows a general flowchart for the training process. Such a hierarchical approach has been used previously for building classical and tight-binding models [42–44] but its potential for constructing NN sets has not been explored. The rest of this paper is organized as follows: Section II details the employed data generation protocol; Section III reviews the descriptors used in this study; Section IV gives the NN setup basics; Section V introduces the stratified training scheme; Section VI illustrates the performance of the NNs for Cu, Pd, Ag, Cu-Pd, Cu-Ag, Pd-Ag, and Cu-Pd-Ag systems; finally, Section VII summarizes our findings and outlooks.

II. GENERATION OF TRAINING DATASETS

Accuracy and diversity of the data created for NN training are among the defining factors in the NN overall performance. It is important to note that developed models inherit the *systematic* errors of the method chosen to calculate structures' total energies, forces, and stresses. Chemically accurate "post-Hartree-Fock" methods have been used in some studies [45, 46] but DFT approximations have been a practical choice for producing reference values for large data sets. The well-known DFT limitations to accurately describe the interactions in strongly correlated or van der Waals systems can be mediated with the DFT+U [47, 48] and the vdW-DF-based [49, 50] approaches with little additional computational cost [51–53]. In some seemingly ordinary cases, such as the Cu-Au binary, obtaining proper values of formation energies requires considerably more expensive hybrid functional-level calculations [54].

For the purpose of investigating the performance of NNs as interatomic models, all training and testing have been performed on data evaluated at the same level of DFT approximations. We used the Perdew-Burke-Ernzerhof (PBE) exchange-correlation functional [55] within the generalized gradient approximation (GGA) [56] and projector augmented wave potentials [57] available in VASP [58, 59]. The 500 eV energy cutoff and dense k-meshes, $N_{k1} \times N_{k2} \times N_{k3} \times N_{atoms} \geq 4,000$ [60], ensured numerical convergence of the formation energy differences to typically within 1-2 meV/atom.

Generation of diverse structures sampling relevant regions of the configuration space is critical for training of NNs because of their notoriously poor function as extrapolators [61]. Previously proposed strategies include running molecular dynamics (MD), creating regular meshes of crystal structure parameters, selecting specific desired geometries, etc. [62–64]. The MD-based approach has the advantage of sampling commonly accessible physical states. However, systems simulated with standard MD tend to remain in low free-energy basins and configurations along MD trajectories tend to correlate. A number of algorithms have been developed that force systems to explore larger regions of the phase space and that enable selection of more dissimilar structures [24, 40, 63, 65, 66]. In particular, an iterative MD-based training protocol proposed in Ref. [63] diversifies training sets by identifying and adding structures for which pre-trained NNs differ the most.

Fig. 2(c) illustrates a shortcoming in the MD-based generation of reference data involving small structures with fixed lattice constants. Heating up small supercells of low-energy structures is an attractive and cost-efficient way of sampling relevant potential energy funnels. However, examination of the pair distribution function reveals an unwanted bias related to the appearance of the same nearest neighbor distances in all such structures. The area under the sharp peak at 5.2 Å in the $2\times2\times2$ 8-atom fcc supercell makes up 15% of the total pair distribution function integrated up to 6 Å. It is desirable to circumvent the occurrence of such biases without expanding the structure size. Variable-cell MD is one possible solution but it is also desirable to avoid long DFT runs even if performed at reduced accuracy settings.

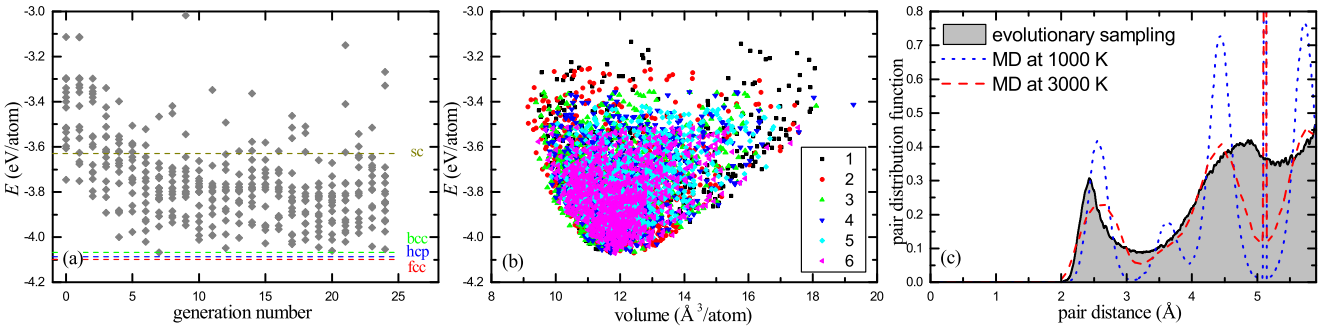

FIG. 2: (color online) Automatically generated structure set for Cu. (a) A typical distribution of energies for a 16-structure population over 25 generations. Dashed lines show energies for select high-symmetry structures. (b) Total distribution of energies versus volume for unit cells with 1 to 6 atoms. (c) Pair distribution function for 1-6 atom structures (shaded gray) and for 3×10^4 8-atom structures in $2 \times 2 \times 2$ fcc supercells in MD runs at different temperatures (non-shaded lines).

We used the following guidelines in designing an alternative protocol: (i) avoid manual selection of structures; (ii) favor low-energy structures; (iii) ensure diversity; and (iv) find representative samples commonly seen in global structure searches. These criteria are satisfied well in mock unconstrained optimization runs driven by an evolutionary algorithm available in our module for *ab initio* structure evolution (MAISE) package [67]. The key differences from real evolutionary structure searches are that we (i) allow only a few steps in local conjugate-gradient optimizations; (ii) apply mutation operations only (distortions of atomic positions and lattice vectors); (iii) use relatively short runs. As can be seen in Fig. 2, these measures have been found to promote sampling of low-energy structures while our previously developed elimination of similar structures based on radial distribution functions [68, 69] maintained diversity in the evolved populations. Both the low-accuracy conjugate-gradient relaxations and the high-accuracy single-point calculations were done at the DFT level. Effectively, the evolutionary sampling protocol is close to a Monte-Carlo-type algorithm where the fitness factor plays the role of the proposal acceptance distribution and where the automated generation of random initial structures helps avoid biases.

For elemental systems we used unit cells with 1-6 atoms; two randomly initialized populations of 16 structures were evolved over 20 generations. For binary and ternary systems we selected different compositions with up to 10 and 6 atoms per unit cells, respectively. After discarding 10% of highest-energy structures in each run we obtained about 8,500, 7,500, and 9,000 structures for unary, binary, and ternary systems, respectively. Table I summarizes the number of data and the standard deviation in each dataset. Fig. 2(c) shows a wider dispersion of interatomic distances in the generated set compared to the MD sets with larger but fixed unit cells. The variable-cell evolutionary sampling eliminates the artificial sharp feature and spreads out peaks from further neighbor shells seen in the MD profile even at temperatures above melting.

It should be acknowledged that the use of small-atom cells invariably imposes certain constraints. For example, atomic environments in 1-atom structures are defined by only 6 parameters. Our following tests indicate no apparent significant consequences for the description of properties in the sampled regions from the presence of the implicit biases. As discussed below in Section VI, one issue detected in structure optimization runs with our trained NNs was an occasional occurrence of short-distance configurations when the starting structure already had unphysically short distances. The strategy of adding such local minima to DFT datasets was found to be ineffective, as artificial minima kept occurring even after a few rounds of NN retraining. We found that complementing the original dataset with a few short- and long-distance configurations (elemental fcc, bcc, hcp, sc, dimer, and square as well as binary $L1_2$, B2, and dimer equilibrium structures scaled by up to $\pm 30\%$) alleviated

Dataset	stratified NN			full NN		
	ΔE	# of	# of	ΔE	# of	# of
	eV/atom	data	weights	eV/atom	data	weights
Cu	0.5172	8551	431	–	–	431
Pd	0.6262	8487	431	–	–	431
Ag	0.4481	8533	431	–	–	431
CuPd	0.5975	7623	1040	0.5829	24661	1902
CuAg	0.5391	7617	1040	0.6601	24701	1902
PdAg	0.5989	7601	1040	0.6833	24621	1902
CuPdAg	0.2170	8917	660	0.6227	57329	5073

TABLE I: A breakdown of datasets and NN adjustable parameters used in stratified and full training. Standard deviations (ΔE) were found individually for each unit cell size and then averaged over the specified dataset. For example, the full CuPd dataset comprises all Cu structures with 1-6 atoms, all Pd structures with 1-6 atoms, and all Cu-Pd structures with 2-10 atoms; the CuPd dataset for stratified training comprises only the binary structures.

the problem while having little influence on the NN overall performance (Section VI). Discarding starting configurations with interatomic distances below 70% of the equilibrium ones ensured robustness of NN-based evolutionary ground state searches.

III. ATOMIC ENVIRONMENT DESCRIPTORS

The description of interatomic interactions with both classical potentials and NNs begins with breaking down the total energy into atomic energies which defines the models' linear scaling with system size. In the case of NNs, the representation of atomic environments has to satisfy the following critical constraints: the NN input needs to have a constant number of components and be invariant to translations, rotations, and identical atom swaps [23]. The first constraint is a considerable challenge because the number of nearest neighbors within a typical 6-Å sphere can change, for instance, from over 70 in close packed bulk structures to about half of that in surface geometries. Elegant solutions for parsing arbitrary chemical environments into NN input vectors include the smooth overlap of atomic positions (SOAP) [23] and Parrinello-Behler (PB) symmetry functions [36].

In this study we have tested and used sets of pair (G^1) and triplet (G^2) PB symmetry functions:

$$G_i^1 = \sum_{j\neq i}^{all} e^{-\eta(R_{ij}-R_s)^2} f_c(R_{ij}), \tag{1}$$

$$G_i^2 = 2^{1-\zeta} \sum_{j,k\neq i}^{all} (1+\lambda\cos\theta_{ijk})^\zeta \times \tag{2}$$
$$e^{-\eta(R_{ij}^2+R_{ik}^2+R_{jk}^2)} f_c(R_{ij}) f_c(R_{ik}) f_c(R_{jk}).$$

The cutoff function $f_c(R_{ij})$ is $0.5\times(\cos(\pi R_{ij}/R_c)+1)$ for $R_{ij} \leq R_c$ and 0 otherwise. The explicit values for R_c, R_s, η, ζ and λ parameters are given in the Supplementary Material [70]. We have found little sensitivity of the resulting errors to the R_c values in the 5-7 Å range for the Cu-Pd-Ag systems. The tests discussed in Section VI indicate that the previously used set of 30 PB symmetry functions provides a fairly good description of considered geometries while keeping the number of input components reasonably low. The latter feature is important for description of mulitcomponent systems because the number of NN adjustable weights is almost linearly dependent on the length of the input vector.

IV. NN SETUP

We have implemented two widely used NN architectures: radial basis functions (RBF), and multilayer perceptron (MLP). The former was shown previously to provide good description of many-body effects for near-equilibrium graphite configurations [35]. However, RBF sets with up to 1,000 Gaussians functions have shown inferior performance for arbitrary geometries in elemental Cu, Pd, and Ag systems. All NN results for multicomponent systems reported in this study have been obtained with two-layer perceptrons.

For an atomic environment of atom i, the N_0 symmetry functions $G_{n_0}^i$ are first rescaled into $x_{n_0}^i$ components of the input vector as discussed below. The inputs and one bias b_0 are then weighted, summed up, and transformed via nonlinear activation functions $f(x) = \tanh(x)$ by N_1 first-layer neurons:

$$x_{n_1}^i = f\left[\sum_{n_0}^{N_0} w_{n_0,n_1}^{(0)} x_{n_0}^i + b_{n_1}^{(0)}\right].$$

The neuron outputs and the first-layer bias b_1 are processed in a similar way by N_2 second-layer neurons:

$$x_{n_2}^i = f\left[\sum_{n_1}^{N_1} w_{n_1,n_2}^{(1)} x_{n_1}^i + b_{n_2}^{(1)}\right].$$

Finally, the resulting values are added up to be the NN energy output:

$$E_i = \sum_{n_2}^{N_2} w_{n_2}^{(2)} x_{n_2}^i + b^{(2)}.$$

The standard way of training such NNs involves the adjustment of weights and biases to minimize the squares of the errors between target and NN-produced values [71]. The known complication in training NN models is that only the *total* rather than *atomic* energies are available in quantum-mechanical calculations [35, 36, 38]. The local information can be introduced in the form of the atomic forces but they do not define the last-layer biases and are more prone to numerical noise. Both energy- and force-based fittings have been discussed and used in previous studies [35, 61, 63, 72]. We have implemented analytical derivatives for each fitting type and rely on either Broyden-Fletcher-Goldfarb-Shanno (BFGS) or conjugate-gradient minimizer to drive the least squares optimization. All presented results have been obtained with total energies as target values.

A preventive measure against favoring certain input components is to determine the full ranges of the symmetry functions in the training set and rescale them to be between -1 and 1. It is a good practice to start with NN weights that make neurons' inputs have the average of 0 and the standard deviation of 1 in *all* layers because very large initial values of x result in small derivative values of the $\tanh(x)$ activation function and, ultimately, in a slow or suboptimal weight convergence [73]. We have adopted a common approach for random initialization of weights ensuring good starting values for all x.

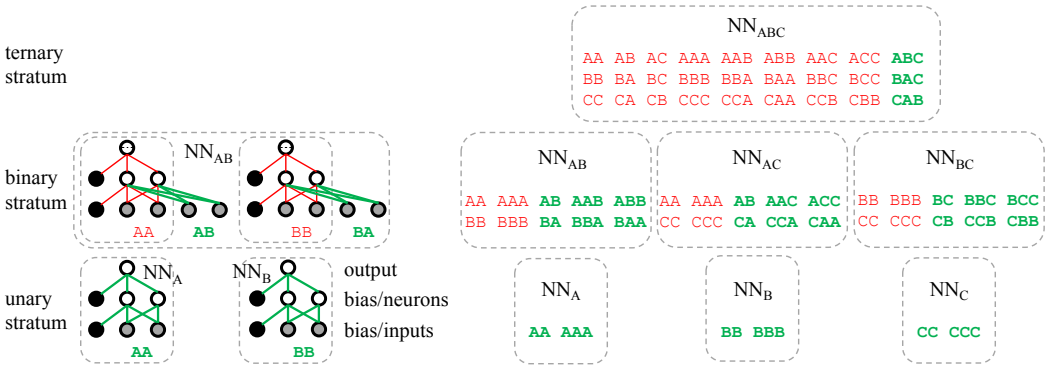

(a) NNs for unary/binary with pair inputs only (b) NNs with shared parameters for unary/binary/ternary systems

FIG. 3: (color online) Schematic representation of stratified training of multilayer NNs. In (a) we show only one hidden layer of neurons and only pair input symmetry functions. Weights and element species shown in bold green are adjusted while the ones in thin red are kept fixed during the training from the bottom up. The letters denote species types in the input vector; for example, AAB describes a triplet symmetry function centered on an A-type atom with A-type and B-type neighbors (the order of neighbors is irrelevant).

V. STRATIFIED TRAINING FOR MULTICOMPONENT SYSTEMS

NNs can and have been successfully used for modeling multicomponent systems but it should be kept in mind that the total number of parameters grows rapidly with the number of elements (see Table I). The formalism generalization requires an extension of symmetry function definitions to multiple element types, specification of NN links to new input components, selection of the training procedure, etc. In a previous study by Artrith et al. [40], a ternary NN for Cu-ZnO trained on a combined set of unary, binary, and ternary data displayed a good performance for elemental systems [40]. The finding is encouraging but NNs for new multicomponent systems would need to be constructed from scratch and would give close but not identical values for shared subsets of elements.

The central question investigated in this study is whether multicomponent NNs could be built from the bottom up and whether they would still be accurate. The procedure shown in Fig. 1 illustrates how separate datasets can be used to optimize the corresponding weights in a natural sequential order. For example, AB binary parameters are trained to the AB database only after A and B elemental parameters are fitted to the A and B databases. Such a hierarchical approach to fitting parameters has been previously used to build semi-empirical models, such as Gupta-type potentials [44, 74], (M)EAM-level potentials [75, 76], and tight-binding models [43]. Here we examine the applicability of the stratified fitting strategy in the context of NNs.

The implementation of the scheme is fairly straightforward provided that two points are handled properly. The first one concerns defining the ranges for interspecies symmetry functions. One needs to ensure that when A-type atoms have no B-type neighbors the NN 'AB' input components $x^i_{n_0}$ are strictly 0. However, the minimum value $G^{min}_{n_0}$ for an AB symmetry function in the full AB binary database might not be 0 because all atoms of species A happened to have at least one neighbor of species B. Then even for a purely A-type structure the non-zero AB-type $x^i_{n_0} = (0 - G^{min}_{n_0})/(G^{max}_{n_0} - G^{min}_{n_0})$ will produce an artificial contribution to the total energy. In all generated databases the $G^{min}_{n_0}/G^{max}_{n_0}$ ratios turned out to not exceed 0.4 and a simple solution to set all $G^{min}_{n_0}$ values to 0 has been found to work well.

The second point concerns specifying which subsets of parameters are allowed to vary in the stratified training. One needs to ensure that a multicomponent NN fitted to the corresponding database produces unchanged output values for constituent elemental/binary structures. Fig. 3(a) helps illustrate that the requirement is met if only the weights connected to the interspecies inputs are allowed to adjust. The input bias weights, in particular, should not be changed because they define the reference energy of a free atom under the previously discussed condition of $G^{min}_{n_0} = 0$ for all $n_0 = 1, \ldots, N_0$.

The following benchmark results illustrate the performance of NNs trained in the standard and stratified fashions. The tests were designed to allow comparisons for practical sizes of datasets and NN parameters that can be generated in future studies for a large set of systems.

VI. RESULTS

A. Total energy errors

In all considered cases we have kept the data to parameter ratio above 7:1 to avoid overfitting. We found the residual and testing errors to differ by less than 5%

	Cu		Pd		Ag		CuPd		CuAg		PdAg		CuPdAg	
	train	test	train	test	train	test	train	test	train	test	train	test	train	test
$NN^{strat.}$	3.88	3.96	10.49	10.91	4.08	3.92	7.06	7.37	3.56	3.84	5.52	6.21	6.45	6.28
NN^{full}_{CuPd}	4.72	4.85	11.16	10.84	–	–	7.07	7.67	–	–	–	–	–	–
NN^{full}_{CuAg}	4.63	4.84	–	–	4.56	4.48	–	–	3.91	4.13	–	–	–	–
NN^{full}_{PdAg}	–	–	11.06	11.25	4.79	4.63	–	–	–	–	5.91	6.05	–	–
NN^{full}_{CuPdAg}	5.24	5.27	11.32	11.45	4.97	4.87	7.83	8.12	4.31	4.43	6.12	6.57	6.36	6.70

TABLE II: Training and testing errors in meV/atom for different systems, evaluated by NNs trained in full and stratified fashions.

in cross validation or random selection tests with 10% of data allocated for this purpose. In order to select a suitable descriptor size and a sufficient number of NN parameters for the analysis of multicomponent systems we first examined the dependence of the testing error on these settings for the Cu, Pd, and Ag elemental systems.

Fig. 4 shows the accuracy of the total energy description using N_0-N_1-N_2-1 NNs with N_0 =8, 30, or 51 PB symmetry functions and $N_1 = N_2$ =10, 14, or 20 neurons. The 30 and 51 sets have been used previously in the investigation of elemental systems [63]. We also considered a subset of only 8 G^1-type pair symmetry functions to illustrate the importance of many-body interactions in these systems. For NNs with the same number of neurons, $N_1 = N_2 = 10$, the inclusion of G^2-type triplet symmetry functions led to substantial drops in the error for Cu, Pd, and Ag by 43%, 10%, and 45% at 30 components and another 20%, 28%, and 5% at 51 components.

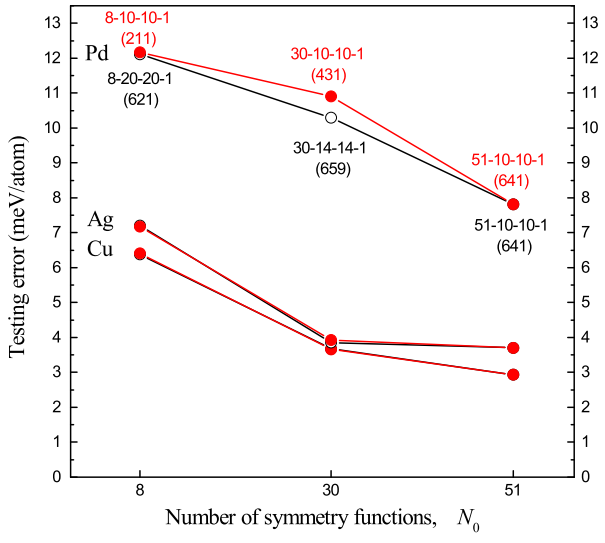

FIG. 4: (Color online) Testing error as a function of number of symmetry functions and NN parameters. The red solid points correspond to N_0-10-10-1 NNs while the black open points correspond to NNs with varying numbers of neurons chosen to be close to the total number of adjustable parameters for different N_0. A noticeable decrease in the testing error is seen only for Pd and $N_0 = 30$.

Since variations in the descriptor size affect the number of NN adjustable parameters, we repeated the tests for 8 and 30 components using $N_1 = N_2 = 20$ and $N_1 = N_2 = 14$ components, respectively. The black points in Fig. 4 correspond the NNs with fairly matched total numbers of free parameters. The little improvement over the N_0-10-10-1 results reveals that the accuracy is defined predominantly by the completeness of the symmetry function sets for these systems.

The considerably higher errors for Pd are only partially explained by the larger standard deviations in the generated datasets (Table I). Given that the PB symmetry functions are fairly general and that the Pd and Ag are of similar size, the different NN performance likely arises from the different complexities of the potential energy surfaces. Our preliminary tests carried out with the same settings for neighboring elements in the periodic table suggest that the accuracy observed for Pd is more of a rule rather than an exception.

Overall, the 30-10-10-1 choice for elemental NNs ensures reasonably good accuracy and keeps the number of parameters relatively low. Non-elemental systems were consequently modeled with 82-10-10-1 binary and 156-10-10-1 ternary NNs. For benchmarking purposes we first employed the standard training approach to generate all combinations of elemental, binary, and ternary NNs for Cu, Pd, and Ag (we use NN^{full}_{AB} and NN^{full}_{ABC} notations to refer to NNs with the full sets of parameters adjusted in the binary and ternary cases, respectively). For example, for the CuPd binary we used 8551 Cu, 8487 Pd, and 7632 CuPd structures and optimized all 1902 parameters in the 82-10-10-1 NN. Merging sets with similar data/parameter ratios should keep the average errors close but the transfer of errors could be a cause for concern. Namely, in the minimization of the total error function the Cu-Cu weights are defined not only by Cu environments in Cu and Cu-Pd structures but also, indirectly, by Pd environments in Cu-Pd and Pd structures.

It has been shown previously that a full training of the Cu-ZnO ternary NN produced a reasonably good elemental Cu model [40]. Systematic tests summarized in Table II indicate that the error transfer is fairly small for the subsystems in our multicomponent NNs as well. For instance, the largest increase in the testing error, from

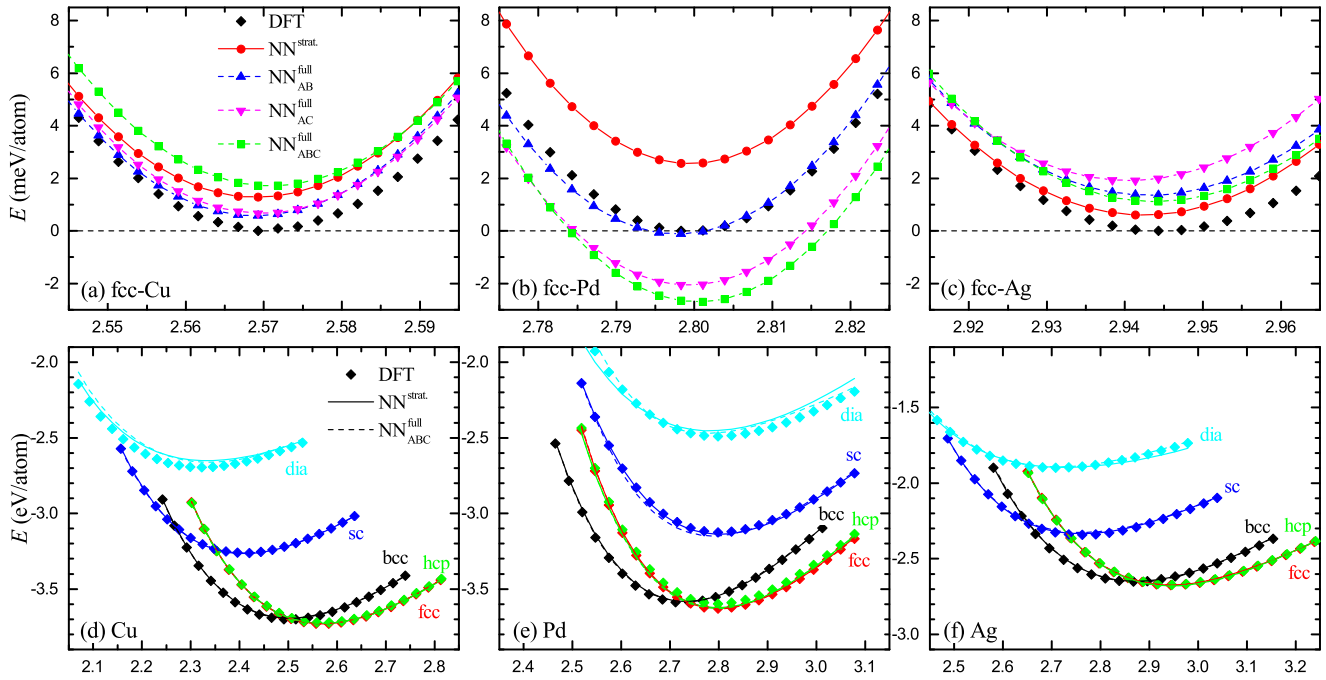

FIG. 5: Total energy as a function of nearest neighbor distance evaluated with DFT and NNs for Cu, Pd and Ag. The top panels show data for the fcc ground states near equilibrium; the colors and types of connected symbols denote the NN flavors. The bottom panels show results for different structures in a wider nearest neighbor distance range; here the solid and dashed lines denote the stratified and full ternary NNs while the colors and types of symbols mark structure types.

3.96 meV/atom with $\mathrm{NN}^{\mathrm{strat.}}$ up to 5.27 meV/atom with $\mathrm{NN}^{\mathrm{full}}_{\mathrm{CuPdAg}}$, is observed for Cu since the model accuracy for this element is influenced in the full training by the lower accuracy of the Pd and Ag descriptions. Judging by the testing errors across all considered systems, the performance of the stratified NNs is comparable to or better than that of the standard NNs.

Fig. 5 details how the NNs constructed in different fashions fair against each other and the DFT data for select high-symmetry structures. Our data generation protocol favored the sampling of configurations around low-energy states (see Fig. 2). Hence, it is not unexpected to see good description, within 2-3 meV/atom, of the fcc ground states in Fig. 5(a-c) which is important for calculation of defect energies and phase diagrams. On a larger scale shown in panels (d-f), it is satisfying to see a good behavior of all NNs even for the high-energy diamond configurations unnatural for these metals. Fig. S1 demonstrates that all these structures are described very well with NNs trained without the bcc, fcc, hcp, and sc equation of state data. In fact, the extra set included to sample short-distance configurations caused a shift away from the ground state energy around the equilibrium distance.

B. Defect formation energies

Evaluation of defect energies is one of the most revealing tests of NN performance because the unit cells generated and used for training are not sufficiently big to simulate defect environments. Vacancy and substitutional defects were calculated in medium-sized bcc, fcc, hcp, and sc supercells. As common in such comparisons, only the atomic positions in the supercells were optimized at the DFT level while the lattice constants were kept fixed at DFT-optimized values. The vacancy formation energies of 0.96, 1.16, and 0.77 eV/vacancy evaluated with DFT in $3 \times 3 \times 3$ 26-atom fcc supercells for Cu, Pd, and Ag were close to respective previously reported DFT values of 0.99, 1.21, and 0.73 eV/vacancy [77]. The NN energies, as in all our tests, were compared for the final structure optimized with DFT but we also checked that following atomic relaxations with NNs resulted in energy gains less than 0.01 eV/defect.

Fig. 6 summarizes the defect formation energy results for all constructed NNs. It can be seen that the type of training had little effect on how the NNs reproduce the DFT values. The accuracy of all Cu-Ag NNs is fairly good in these tests, typically within 10-30% of $E^{\mathrm{defect}}_{\mathrm{form}}$. For the defect structures involving Pd, the NNs display noticeable deviations reaching 0.4 eV/defect. Surprisingly, the largest errors occurred when the substitution of Ag for Pd in the fcc matrix is evaluated with $\mathrm{NN}^{\mathrm{full}}_{\mathrm{PdAg}}$

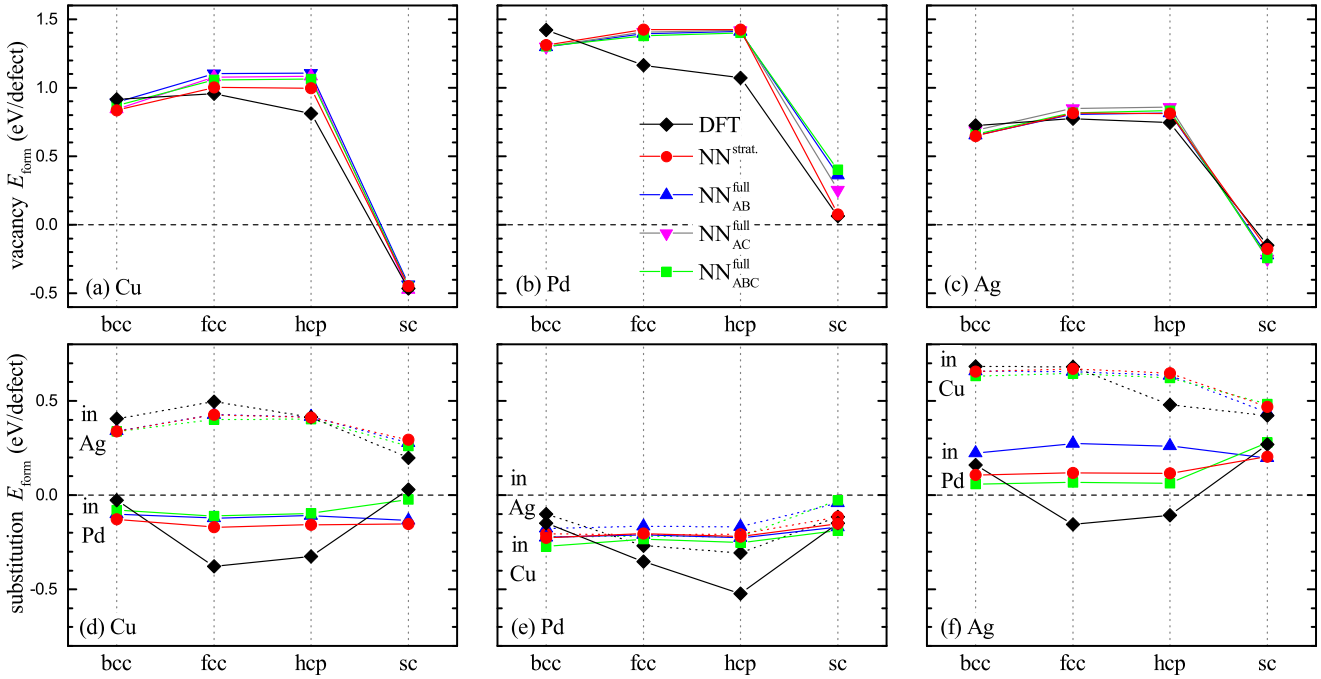

FIG. 6: Defect formation energies in high-symmetry Cu, Pd, and Ag structures evaluated with DFT and different NNs. The top and bottom panels correspond to vacancy and substitutional defects, respectively. In (d-f), the solid and dotted lines are used to differentiate into which ideal elemental lattice an atom is embedded; e.g., in (d) Cu replaces either Ag or Pd atoms.

specifically tuned to this binary. The 0.2-0.4 eV/defect discrepancies are not unexpected because these values, calculated per *unit cells* of about 30 atoms, correspond to $\sim$ 10 meV/atom errors. It is still worth examining how different factors affect the NN performance in this case.

A widely discussed issue is that the scope of NN applicability extends as far as the dataset does. In particular, simulation of structures with any of the symmetry function values outside of the sampled range corresponds to the NN extrapolation regime and is not expected to produce reliable outputs [61]. Fig. 7 illustrates that creation of a vacancy in the $3 \times 3 \times 3$ 27-atom fcc-Pd causes small deviations of atomic environments from the ideal one when compared to the distribution of input values in the full elemental Pd dataset. However, even if all input components of new structures to be evaluated are between the corresponding minimum and maximum values of the training set the points could be far away from any data clusters in the large N_0-dimensional configuration space.

Addition of the Ag-in-fcc-Pd defect structure into the training set reduced the 0.27 eV/defect discrepancy between DFT and NN$^{strat.}$ down to 0.25, 0.18, and 0.02 eV/defect if the data point was weighted by a factor of 10, 100, and 1000, respectively. For comparison, increasing the number of descriptor components to 51 reduced the error down to 0.22 eV/defect. Clearly, describing the defect energy better than 0.1 eV/defect is difficult given the $\sim$4-7 meV/atom overall accuracy of the constructed NNs.

C. Compound formation energies

Accurate evaluation of compound formation energies is a critical benchmark for the developed models to be used for materials prediction. The sign determines the miscibility of elements while the magnitude determines which compositions are thermodynamically stable via construction of the convex hull [78]. The absolute values of the formation energy in the considered binaries are relatively low, about 100 meV/atom but high enough to be resolved with NNs.

For our first test, we considered fcc and bcc solid solutions common in these binaries. As described in the

binary	ΔE in meV/atom			
	NN$^{strat.}$	NN$^{full}_{AB}$	NN$^{full}_{ABC}$	DFT$_{relaxed}$
CuPd	7.5	5.7	6.6	1.3
CuAg	6.0	5.6	6.0	0.8
PdAg	11.7	8.1	9.7	0.9

TABLE III: Column (1) Binary systems investigated with unconstrained evolutionary searches as described in the text. Columns (2 and 3) Formation energy errors in 3 sets of 8-atom binary structures identified in evolutionary searches (see Fig. 7). Column (4) Average gain in energy after local relaxations of NN-optimized structures with DFT.

Supplementary Material [70], we simulated the alloys in known special quasirandom structures [79–81] and in our own sets of 8- and 16-atom random structures. The average errors for these phases were lower than the corresponding NN errors by 1-2 meV/atom in nearly all cases which can be expected for the well-sampled low-energy part of the configurational space (Fig. S2).

In order to generate a more diverse test set of binary structures and check the robustness of the trained NNs we performed a series of NN-based evolutionary ground searches. For the three binaries, we considered $A_{8-n}B_n$ ($n = 1 \ldots 7$) compositions and used a typical set of evolutionary settings from our previous DFT-based searches [68, 69]. 16 member in populations were evolved over 50 generations, as 70% and 30% of children were created with crossover and mutation operations, respectively. The former involved mixing of approximately halves of two parent structures and the latter consisted of lattice distortions, atom displacements, and atom swaps. The most stable structure was typically found within the first 10 generations. The number of structures detected to have short interatomic distances at the beginning of or during local optimizations was small, 0.4%, 0.1% and 4.4% for CuPd, CuAg, and PdAg, respectively.

An important outcome of these simulations summarized in Fig. 8 is that the developed interpolation-type models with numerous parameters showed no clearly unphysical low-energy configurations. A similar behavior was observed in evolutionary runs for the elemental and ternary systems (not shown). The formation energy differences calculated with DFT and NN for the sets of 7 binary lowest-energy structures in Table III correlate well with the NNs testing errors in Table II. Note that because $E_{\rm form}(A_{1-x}B_x)$ is defined as $E(A_{1-x}B_x) - (1-x)E(A) - xE(B)$ the reference energy errors for the elements add to the total formation energy errors. $\mathrm{NN}^{\rm full}_{\rm AB}$ tuned to the corresponding binaries are in sligthly better agreement with DFT than $\mathrm{NN}^{\rm strat.}$ or $\mathrm{NN}^{\rm full}_{\rm ABC}$.

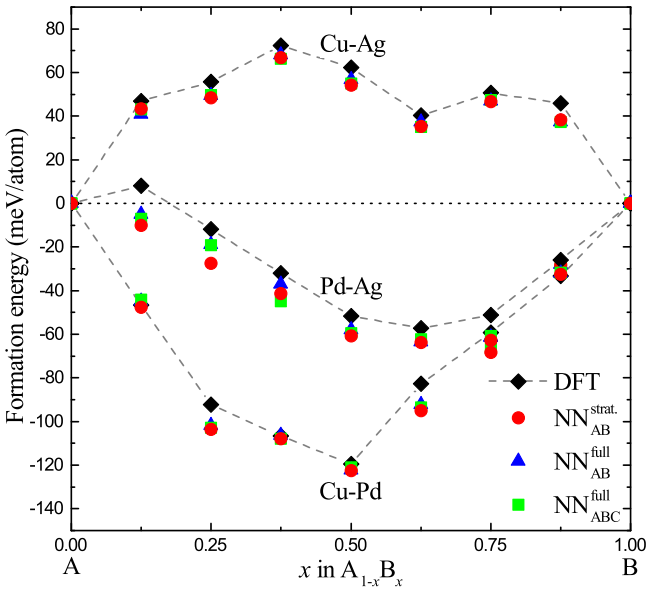

FIG. 8: Formation energies calculated with NN and DFT methods for lowest-energy 8-atom binary structures found in evolutionary searches based on $\mathrm{NN}^{\rm strat.}$ interatomic models. The dotted lines are a guide for the eye.

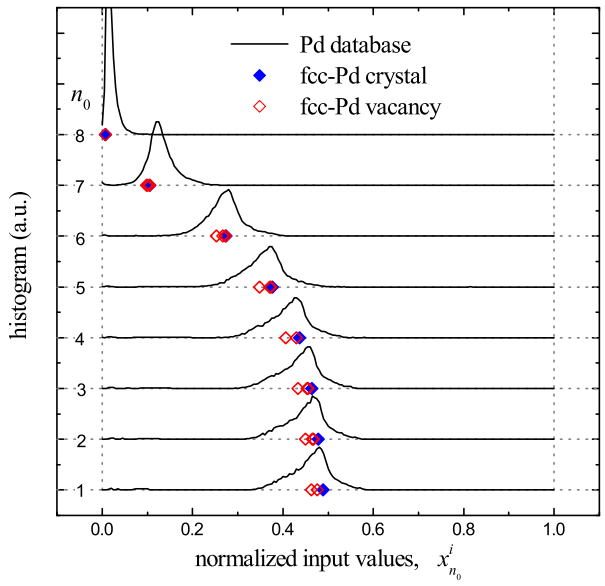

FIG. 7: Distribution of normalized input components in the full Pd database and select structures. Creation of a vacancy in the $3 \times 3 \times 3$ 27-atom fcc-Pd supercell results in 3 Wyckoff sites. The input values corresponding to their atomic environments are close to the ideal ones in fcc-Pd and to the middle of distribution peaks (only the first 8 pair-symmetry function values are shown for clarity). The sites contribute to $E^{\rm vac}_{\rm form} = 1.42$ eV as follows: $12(0.210) + 8(-0.072) + 6(-0.087)$ eV.

The largest deviations for all three NNs happened in the Pd-Ag binary at the Pd-rich end, the composition limit with the least accurate description of the substitutional defect energies in Fig. 6. Notably, the NN results were consistently below the corresponding DFT values rather than scatter around them. Because of this trend, relative energies calculated needed for the construction of a convex hull should be more accurate. Nevertheless, a reliable identification of thermodynamically stable alloys at different stoichiometries requires resolution of relative energies typically with 1-2 meV/atom accuracy which is difficult to achieve. It is important, however, that the relaxed crystal structures produced with the NN-based evolutionary searches are very close to local minima in the DFT treatment, as additional DFT-based relaxation lowers the energy by about only 1 meV/atom (Table III). Hence, NN-based searches can provide a pool of viable candidates that can be quickly tested at the DFT level.

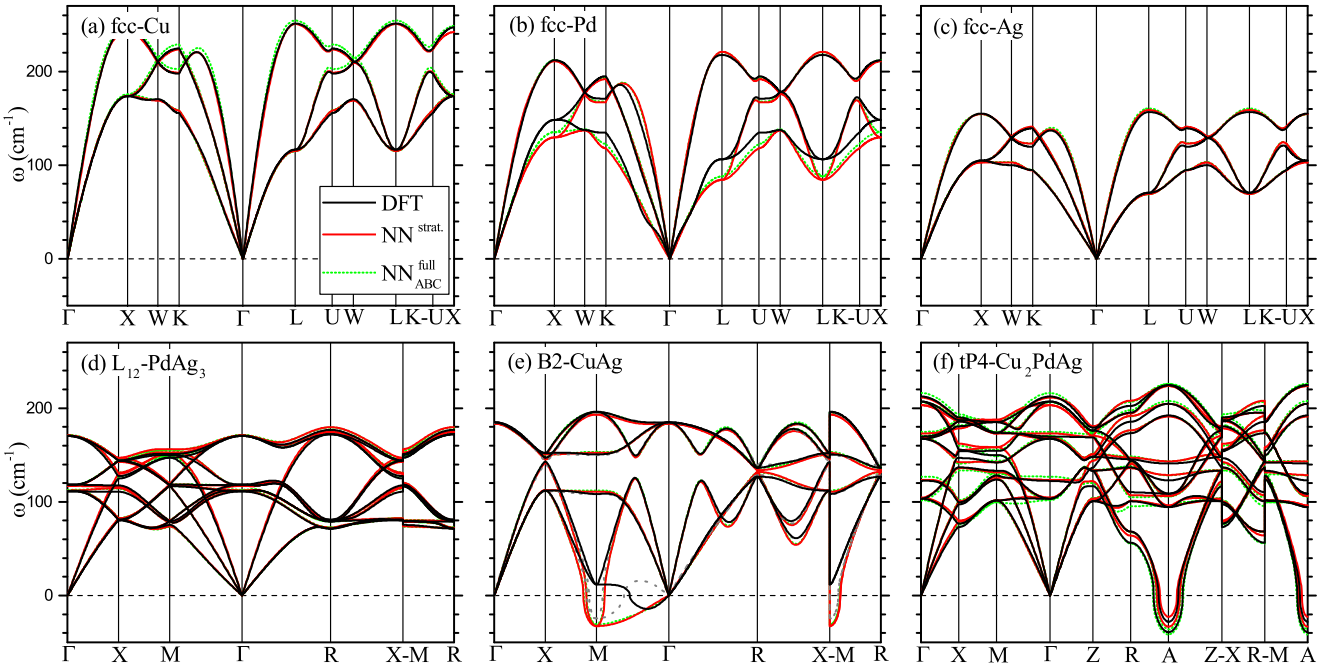

FIG. 9: Phonon dispersions calculated with the frozen phonon method at the DFT, stratified NN, and full NN levels. The dotted gray lines in (e) illustrate the change in the soft-mode frequencies calculated with DFT when the supercell size is reduced from $4 \times 4 \times 4$ to $3 \times 3 \times 3$.

D. Phonons

Evaluation of atomic-force defined quantities gives valuable information about classical models because the derivatives depend on neighbors twice the cutoff distance away from the considered atom [35]. We used the frozen phonon method as implemented in PHON [82] to calculate force constants and phonon dispersions for representative structures. The same supercells (above 108 atoms) and settings (displacement size 0.04 Å) were used in DFT and NN calculations. Dispersions were plotted along high-symmetry directions as defined in Ref. 83.

The top panels in Fig. 9 show phonon frequencies calculated with the help of $6 \times 6 \times 6$ expansions of primitive fcc cells using DFT (black), stratified NN (red), and full NN (green) methods. We observe essentially no difference between the results obtained with the two types of NNs and an excellent agreement with the DFT data. As in the other tests, the most noticeable deviations (for some optical modes) are seen in the challenging Pd case. The acoustic modes are reproduced well even for Pd which can be attributed to insignificance of constant energy shifts, shown in Fig. 9, in the calculation of derivatives.

The bottom panels in Fig. 9 show phonons in multicomponent structures based on fcc (d,f) and bcc (e). Again, the two NN types produce very similar dispersions remarkably close to the DFT curves in (d) and (f). It is satisfying to see that the NNs captured the large softening of certain modes and the presence of imaginary frequencies shown as negative values in (e) and (f). The discrepancy for the lowest M-point frequencies in (e) is not surprising due to the known sensitivity of phonon results to simulation settings at the DFT level [84, 85]. For instance, by reducing the supercell from $4 \times 4 \times 4$ to $3 \times 3 \times 3$ in which the M-point is not folded onto Γ we obtained a very different shape of the lowest phonon branch along $\Gamma - M$ with DFT; in contrast, the dispersions calculated in the smaller supercell with the NNs were essentially unchanged. Further tests in the Supplementary Material [70] (Fig. S3) illustrate the difficulty of obtaining converged DFT results. Nevertheless, it is evident that the phonon softening magnitudes with respect to the 110 cm^{-1} unsoften mode frequency at the M point in Fig. 9(e) are comparable in the two treatments: ~ 100 cm^{-1} with the DFT and ~ 140 cm^{-1} with the NN. The observed ability of the NNs to identify dramatically softened modes is crucial for constructing dynamically, and possibly thermodynamically, stable derivatives in structure searches.

Another important use of NNs is inclusion of vibrational entropy contributions to the free energy at finite temperatures [82]. Given the generally good agreement for the phonon modes along the high-symmetry directions, one could expect a reasonably accurate estimate of the phonon DOS integrated over the full Brillouin zone as well. Using a standard expression $\Delta F = k_B T \int_0^\infty d\omega g(\omega) \ln(2 \sinh(\hbar\omega)/2k_B T)$ [82], we calculated the quasiharmonic corrections at 0 and 1000 K for the 6 considered structures [86]. The zero point energies, found

to be between 20-30 meV/atom in magnitude, were described by the NNs within 0.6 meV/atom of the DFT values for all 6 phases. The corrections went up to 400-500 meV/atom at 1000 K but were still described well with NNs. Table IV illustrates that the mismatches between NN and DFT results remained below 9 meV/atom for the elements. The NNs captured the sign and the magnitude, within 7 meV/atom, of the vibrational contributions to the *formation* free energies for the 3 compounds. The tests suggest that the NN models linearly scaling with system size can be used for a fast examination of compound stability at realistic synthesis conditions.

VII. DISCUSSION AND CONCLUSIONS

Having presented our main results and observations, we expand on our discussion of the NN model robustness, parameter meaning, expected advantages/limitations, and applicability scope.

Development of a robust training procedure requires resulting NNs be not sensitive to the particular weight initialization and choice of the data subsets. During the course of this work, we have constructed over 500 various Cu-Pd-Ag NNs and observed little dependence of the model performance on these factors. Namely, after 60,000 steps of BFGS or conjugate-gradient optimization, the residual and testing errors invariably converged to values within 3-5% of each other. The close accuracy of NNs trained to different data subsets suggest that there are many comparable local minima in the large configuration space of NN parameters. The observation is supported by our additional tests in which we monitored various NN outputs as the models were being tuned. As shown in Fig. S4, we calculated formation energies, phonon frequency, etc., using three differently initialized NNs after every 20,000 training steps. After 60,000 steps, all probed properties converged to very close values in all three cases. It might still be worth trying more advanced error minimization techniques, such as the evolutionary algorithm, but so far we have not observed a particular need for that.

Interpretation of the NN inner workings is notoriously difficult due to the sheer quantity and the hierarchical connectivity of adjustable weights. We looked for possible parameter correlations in simplified one-layer 16-10-1 binary NNs with 8 pair symmetry functions per element. As can be seen in Fig. 3(a), the weights connecting the inputs and the first-layer neurons define the interspecies interaction strength. Suppose all $w_{n_0,n1}^{(0),\mathrm{AA}}$ and $w_{n_0,n1}^{(0),\mathrm{AB}}$ pairs for every symmetry function n_0 were identical; then a substitution of A for B would not change the energies of any neighboring A-type atoms. We trained full and stratified NNs for CuPd, CuAg, and PdAg using 3 different data subsets for each binary (18 NNs in total). Typical distributions of $w_{n_0,n1}^{(0),\mathrm{AA}}$ and $w_{n_0,n1}^{(0),\mathrm{AB}}$ weights plotted in Fig. S5(a,b) do not exhibit particularly strong correlations. After fitting all 36 sets with linear dependences and plotting Pearson's r values in Fig. S5(c) we observed a consistently better correlation of weights in NNs trained in the full fashion, i.e., when AA, AB, BB, BA, and all biases were adjusted simultaneously. Fitted linear slopes were found to be all positive, with angles between 10 and 80 degrees for all trained NNs which indicates an overall tendency for AB and AA parameters to have the same sign. Ideally, one would want to break down the results further by symmetry functions to establish which inputs are most significant for defining interspecies interactions or how to initialize weights for faster convergence. Unfortunately, even for these simplified NNs we could not extract any other noticeable trends.

It is worth clarifying further how weight constraining affects the flexibility of NNs to describe multicomponent systems. Fig. 3 shows that there are no more adjustable parameters beyond the ternary set and it may appear that NNs cannot be tuned to model quaternary systems due to stratification of training. In reality, the limitation is imposed by the use of pair and triplet symmetry functions. Without explicitly including quadruplet symmetry functions to account for 4-body interaction terms, the adjustment of all weights to the full dataset with the standard training would not carry much physical meaning. In this respect, matching data and parameter sets in the stratified approach seems more transparent and justifiable.

The demonstrated good performance of both standard and stratified NNs could be related to the similarity of the considered elements. Treatment of systems comprised of elements with very different bonding mechanisms, such as metal hydrides, oxides, etc., is certainly more challenging [87]. With the top-level weights fixed, the modulation of, e.g., metal AA inputs by metal-hydrogen AB inputs before the net signal is fed into the first-layer neurons might be insufficient to fully capture the hybridization and charge transfer effects between the elements with such differences in size and electronegativity. The actual limitation in both training schemes is due to the adopted linkage of inputs to the first-level neurons only. Since fully trained NN with this architecture have performed well for Cu-ZnO and NaCl [40, 88] systems, one can expect a comparable performance for stratified NNs. A way to relax the architecture-defined constraint for both fitting schemes is to link the inputs to higher-level neurons as well. In fact, generation of reliable DFT data

model	$\Delta F - \Delta F^{\mathrm{DFT}}$			ΔF_{form}		
	Cu	Pd	Ag	CuAg	$PdAg_3$	Cu_2PdAg
DFT	-	-	-	-21.0	6.5	-10.9
$NN^{\mathrm{strat.}}$	0.3	-8.7	2.8	-27.9	9.3	-8.8
$NN^{\mathrm{full}}_{\mathrm{CuPdAg}}$	2.9	-3.9	4.3	-28.2	6.4	-9.5

TABLE IV: Thermal corrections to free energy (elemental sytems) and formation free energy (multielement systems) at 1000 K in meV/atom.

is a greater challenge for strongly correlated transition metal oxides due to the known difficulty of defining the U parameter for the full composition range and obtaining converged DFT+U energies [89, 90].

The computational cost of constructing and using NNs is reasonably low and allows for modeling extended sets of multicomponent systems. The DFT data generation stage requires an initial investment of about 10,000 CPU hours per unary, binary, or ternary set, with roughly one CPU hour per small unit cell sized structure considered in this study. For the described data and parameter set sizes, full NN training takes close to 25 CPU hours for unaries and 600 CPU hours for ternaries. Stratified NN training for a *single* ternary system takes about half the total time ($3 \times 25 + 3 \times 50 + 100 = 325$ CPU hours). More importantly, construction of NN models for new sets of multicomponent systems, e.g., all binary and ternary combinations of 5 elements, should be faster by an order of magnitude. The speed-up is significant even with the efficient parallelization of the training process available in MAISE. As has been pointed out in previous studies [41], NNs are about factor of 100 slower than traditional potentials but offer a considerable speed-up compared to DFT calculations. In our implementation, a single calculation of the energy, forces, and stresses for a 100-atom structure takes a factor of 10^3-10^4 less CPU time with NNs compared to DFT.

It should be noted that while the NN 10-meV/atom accuracy might not be sufficient to definitively resolve identified competing structures in some systems, the coupling of the two bio-inspired algorithms can dramatically reduce the pool of viable candidates that need to be calculated at the DFT level. The structure search acceleration strategy has been used previously in combination with pre-defined or tuned-on-the-fly classical potentials [44]. In the present approach, a system-specific NN can be generated on demand. With the available tests and monitors of the models' transferability, they may be suitable for reuse in future large-scale simulations.

In summary, we have outlined and examined schemes for (i) automated generation of data and (ii) stratified construction of multicomponent NNs which, to the best of our knowledge, have not been previously used in the development of NN-based interatomic models. The employed data generation protocol avoids certain biases present in the MD-based approach and samples parts of the configurational space typically accessed in ground state searches. The use of small-cell structures enables creation of extended databases for fitting NNs with several thousand adjustable weights. The stratified NN training procedure for multicomponent systems is centered on reusing fitted parameters from constituent NNs. Test results for a range of properties showed that the accuracy of produced NNs is maintained for the considered Cu-Pd-Ag system. The sequential fitting of parameters to corresponding element-specific databases has the potential to accelerate the construction of NN libraries and enable a direct comparison of properties, such as formation energies, across chemical element sets. It should be kept in mind that NNs, as any classical interatomic models, are not universally transferable; therefore, unary NNs should be carefully tuned and tested for targeted geometries, e.g., for bulk or nanoparticle structure sets, before they can be expanded to treat the corresponding multicomponent configurations. While NNs have already been used for structure prediction [91, 92], the methodology has yet to be widely adopted. Presented tests indicate that NNs are robust enough to be used in evolutionary ground state searches. With a moderate investment of computational resources to build a NN for a specific alloy, one can explore the full composition range using unconstrained optimizations which can in some cases take over 10^5 CPU hours for a single composition at the DFT level [69]. Viability of the methodology to accelerate structure prediction for a wider range of geometries and chemical systems is subject of our on-going work.

VIII. ACKNOWLEDGMENTS

The authors gratefully acknowledge the NSF support (Award No. DFM-1410514).

[1] A. P. Bartók and G. Csányi, International Journal of Quantum Chemistry **115**, 1051 (2015).
[2] J. Behler, International Journal of Quantum Chemistry **115**, 1032 (2015).
[3] E. B. Tadmor and R. E. Miller (New York : Cambridge University Press, 2011).
[4] T. Liang, Y. K. Shin, Y.-T. Cheng, D. E. Yilmaz, K. G. Vishnu, O. Verners, C. Zou, S. R. Phillpot, S. B. Sinnott, and A. C. van Duin, Annual Review of Materials Research **43**, 109 (2013).
[5] E. B. Tadmor, R. S. Elliott, S. R. Phillpot, and S. B. Sinnott, Current Opinion in Solid State and Materials Science **17**, 298 (2013).
[6] E. B. Tadmor, R. S. Elliott, J. P. Sethna, R. E. Miller, and C. A. Becker, JOM **63**, 17 (2011).
[7] M. Wen, S. M. Whalen, R. S. Elliott, and E. B. Tadmor, Modelling Simul. Mater. Sci. Eng. **23**, 074008 (2015).
[8] R. J. Bartlett and J. F. Stanton, Reviews in Computational Chemistry, Volume 5 pp. 65–169 (2007).
[9] A. Jain, Y. Shin, and K. A. Persson, Nature Reviews Materials **1**, 15004 EP (2016).
[10] R. O. Jones, Rev. Mod. Phys. **87**, 897 (2015).
[11] S. Curtarolo, D. Morgan, and G. Ceder, Calphad **29**, 163 (2005).
[12] A. V. D. Geest and A. Kolmogorov, Calphad **46**, 184 (2014).
[13] J. Tersoff, Phys. Rev. Lett. **56**, 632 (1986).
[14] M. S. Daw and M. I. Baskes, Phys. Rev. Lett. **50**, 1285

(1983).
[15] P. L. Williams, Y. Mishin, and J. C. Hamilton, Modelling Simul. Mater. Sci. Eng. **14**, 817 (2006).
[16] M. Wilson and P. A. Madden, Journal of Physics: Condensed Matter **5**, 2687 (1993).
[17] J. E. Jones, Proceedings of the Royal Society of London A: Mathematical, Physical and Engineering Sciences **106**, 463 (1924).
[18] J. D. Perea, S. Langner, M. Salvador, J. Kontos, G. Jarvas, F. Winkler, F. Machui, A. Görling, A. Dallos, T. Ameri, et al., The Journal of Physical Chemistry B **120**, 4431 (2016).
[19] G. Csányi, T. Albaret, M. C. Payne, and A. De Vita, Phys. Rev. Lett. **93**, 175503 (2004).
[20] A. N. Kolmogorov and V. H. Crespi, Phys. Rev. B **71**, 235415 (2005).
[21] F. Bianchini, J. R. Kermode, and A. D. Vita, Modelling Simul. Mater. Sci. Eng. **24**, 045012 (2016).
[22] T. B. Blank, S. D. Brown, A. W. Calhoun, and D. J. Doren, The Journal of Chemical Physics **103**, 4129 (1995).
[23] A. P. Bartók, R. Kondor, and G. Csányi, Phys. Rev. B **87**, 184115 (2013).
[24] D. A. R. S. Latino, F. F. M. Freitas, J. Aires-De-Sousa, and F. M. S. Silva Fernandes, International Journal of Quantum Chemistry **107**, 2120 (2007).
[25] E. Sanville, A. Bholoa, R. Smith, and S. D. Kenny, Journal of Physics: Condensed Matter **20**, 285219 (2008).
[26] R. M. Balabin and E. I. Lomakina, The Journal of Chemical Physics **131**, 074104 (2009).
[27] W. O. Griffin and J. A. Darsey, International Journal of Hydrogen Energy **38**, 11920 (2013).
[28] K. T. Schütt, H. Glawe, F. Brockherde, A. Sanna, K. R. Müller, and E. K. U. Gross, Phys. Rev. B **89**, 205118 (2014).
[29] R. Jalem, M. Nakayama, and T. Kasuga, J. Mater. Chem. A **2**, 720 (2014).
[30] T. Santos-Silva, P. I. C. Teixeira, C. Anquetil-Deck, and D. J. Cleaver, Phys. Rev. E **89**, 053316 (2014).
[31] G. Pilania, C. Wang, X. Jiang, S. Rajasekaran, and R. Ramprasad, Scientific Reports **3**, 2810 EP (2013).
[32] Z. Li, J. R. Kermode, and A. De Vita, Phys. Rev. Lett. **114**, 096405 (2015).
[33] V. Botu and R. Ramprasad, Phys. Rev. B **92**, 094306 (2015).
[34] J. B. Witkoskie, , and D. J. Doren, Journal of Chemical Theory and Computation **1**, 14 (2005).
[35] A. N. Kolmogorov, Ph.D. thesis, The Pennsylvania State University (2004).
[36] J. Behler and M. Parrinello, Phys. Rev. Lett. **98**, 146401 (2007).
[37] H. Eshet, R. Z. Khaliullin, T. D. Kühne, J. Behler, and M. Parrinello, Phys. Rev. B **81**, 184107 (2010).
[38] W. J. Szlachta, A. P. Bartók, and G. Csányi, Phys. Rev. B **90**, 104108 (2014).
[39] S. Kondati Natarajan, T. Morawietz, and J. Behler, Phys. Chem. Chem. Phys. **17**, 8356 (2015).
[40] N. Artrith, B. Hiller, and J. Behler, physica status solidi (b) **250**, 1191 (2013).
[41] J. Behler, Journal of Physics: Condensed Matter **26**, 183001 (2014).
[42] A. Seko, Y. Koyama, and I. Tanaka, Phys. Rev. B **80**, 165122 (2009).
[43] A. Urban, M. Reese, M. Mrovec, C. Elsässer, and B. Meyer, Phys. Rev. B **84**, 155119 (2011).
[44] S. Núñez and R. L. Johnston, The Journal of Physical Chemistry C **114**, 13255 (2010).
[45] E. Pradhan and A. Brown, The Journal of Chemical Physics **144**, 174305 (2016).
[46] G. Montavon, M. Rupp, V. Gobre, A. Vazquez-Mayagoitia, K. Hansen, A. Tkatchenko, K.-R. Müller, and O. A. von Lilienfeld, New Journal of Physics **15**, 095003 (2013).
[47] S. L. Dudarev, G. A. Botton, S. Y. Savrasov, C. J. Humphreys, and A. P. Sutton, Phys. Rev. B **57**, 1505 (1998).
[48] V. I. Anisimov, J. Zaanen, and O. K. Andersen, Phys. Rev. B **44**, 943 (1991).
[49] J. Klimeš and A. Michaelides, The Journal of Chemical Physics **137**, 120901 (2012).
[50] H. Rydberg, M. Dion, N. Jacobson, E. Schröder, P. Hyldgaard, S. I. Simak, D. C. Langreth, and B. I. Lundqvist, Phys. Rev. Lett. **91**, 126402 (2003).
[51] K. Burke, The Journal of Chemical Physics **136**, 150901 (2012).
[52] G. Hautier, A. Jain, and S. P. Ong, Journal of Materials Science **47**, 7317 (2012).
[53] A. Bil, B. Kolb, R. Atkinson, D. G. Pettifor, T. Thonhauser, and A. N. Kolmogorov, Phys. Rev. B **83**, 224103 (2011).
[54] Y. Zhang, G. Kresse, and C. Wolverton, Phys. Rev. Lett. **112**, 075502 (2014).
[55] J. P. Perdew, K. Burke, and M. Ernzerhof, Phys. Rev. Lett. **77**, 3865 (1996).
[56] J. P. Perdew, K. Burke, and M. Ernzerhof, Phys. Rev. Lett. **78**, 1396 (1997).
[57] P. E. Blöchl, Phys. Rev. B **50**, 17953 (1994).
[58] G. Kresse and J. Hafner, Phys. Rev. B **47**, 558 (1993).
[59] G. Kresse and J. Furthmüller, Phys. Rev. B **54**, 11169 (1996).
[60] H. J. Monkhorst and J. D. Pack, Phys. Rev. B **13**, 5188 (1976).
[61] J. Behler, The Journal of Chemical Physics **134**, 074106 (2011).
[62] S. Lorenz, M. Scheffler, and A. Gross, Phys. Rev. B **73**, 115431 (2006).
[63] N. Artrith and J. Behler, Phys. Rev. B **85**, 045439 (2012).
[64] A. P. Bartók, M. J. Gillan, F. R. Manby, and G. Csányi, Phys. Rev. B **88**, 054104 (2013).
[65] G. A. Tribello, M. Ceriotti, and M. Parrinello, Proceedings of the National Academy of Sciences **109**, 5196 (2012).
[66] A. M. Reilly, D. S. Middlemiss, M. M. Siddick, D. A. Wann, G. J. Ackland, C. C. Wilson, D. W. H. Rankin, , and C. A. Morrison, The Journal of Physical Chemistry A **112**, 1322 (2008).
[67] A. N. Kolmogorov (2009), URL `http://maise-guide.org`.
[68] A. N. Kolmogorov, S. Shah, E. R. Margine, A. F. Bialon, T. Hammerschmidt, and R. Drautz, Phys. Rev. Lett. **105**, 217003 (2010).
[69] A. N. Kolmogorov, S. Shah, E. R. Margine, A. K. Kleppe, and A. P. Jephcoat, Phys. Rev. Lett. **109**, 075501 (2012).
[70] See supplementary material at online address (2016).
[71] C. M. Bishop, Review of Scientific Instruments **65**, 1803 (1994).
[72] A. Pukrittayakamee, M. Malshe, M. Hagan, L. M. Raff, R. Narulkar, S. Bukkapatnum, and R. Komanduri, The

Journal of Chemical Physics **130**, 134101 (2009).
[73] D. Nguyen and B. Widrow, in *Neural Networks, 1990., 1990 IJCNN International Joint Conference on* (1990), pp. 21–26 vol.3.
[74] X. Wu, W. Cai, and X. Shao, Journal of Computational Chemistry **30**, 1992 (2009).
[75] J. Luyten, M. Schurmans, C. Creemers, B. S. Bunnik, and G. J. Kramer, Surface Science **601**, 1668 (2007).
[76] J. Luyten, J. D. Keyzer, P. Wollants, and C. Creemers, Calphad **33**, 370 (2009).
[77] C. Zhang, , and A. Alavi, Journal of the American Chemical Society **127**, 9808 (2005).
[78] S. Curtarolo, D. Morgan, and G. Ceder, Calphad **29**, 163 (2005).
[79] A. Zunger, S.-H. Wei, L. G. Ferreira, and J. E. Bernard, Phys. Rev. Lett. **65**, 353 (1990).
[80] C. Jiang, C. Wolverton, J. Sofo, L.-Q. Chen, and Z.-K. Liu, Phys. Rev. B **69**, 214202 (2004).
[81] C. Wolverton, Acta Materialia **49**, 3129 (2001).
[82] D. Alf, Computer Physics Communications **180**, 2622 (2009).
[83] W. Setyawan and S. Curtarolo, Computational Materials Science **49**, 299 (2010).
[84] E. D. Sandoval, S. Hajinazar, and A. N. Kolmogorov, Phys. Rev. B **94**, 094105 (2016).
[85] W. Gao, T. A. Abtew, T. Cai, Y.-Y. Sun, S. Zhang, and P. Zhang, arXiv:1504.06259 (2015).
[86] The values are not physically meaningful for the dynamically unstable CuAg and Cu_2PdAg phases but allowed us to compare the DFT and NN phonon DOS integrated over the *real* frequency ranges.
[87] J. Behler, Phys. Chem. Chem. Phys. **13**, 17930 (2011).
[88] S. A. Ghasemi, A. Hofstetter, S. Saha, and S. Goedecker, Phys. Rev. B **92**, 045131 (2015).
[89] B. Meredig, A. Thompson, H. A. Hansen, C. Wolverton, and A. van de Walle, Phys. Rev. B **82**, 195128 (2010).
[90] A. Jain, G. Hautier, S. P. Ong, C. J. Moore, C. C. Fischer, K. A. Persson, and G. Ceder, Phys. Rev. B **84**, 045115 (2011).
[91] N. Artrith and A. M. Kolpak, Nano Letters **14**, 2670 (2014).
[92] J. Behler, R. Martoňák, D. Donadio, and M. Parrinello, Phys. Rev. Lett. **100**, 185501 (2008).